International Forum on Aeroelasticity and Structural Dynamics
IFASD 2019
9-13 June 2019, Savannah, Georgia, USA

FUZZY GAIN-SCHEDULING FOR MIMO SYSTEMS APPLIED TO FLEXIBLE AIRCRAFT CONTROL

Guilherme C. Barbosa[1], Antônio B. Guimarães Neto[1], Rafael M. Bertolin[1], Flávio J. Silvestre[2]

[1]Instituto Tecnológico de Aeronáutica
São José dos Campos, São Paulo 12228900 Brazil
guichavesbarbosa@gmail.com
antoniobgn@gmail.com
rafaelmbufsj@gmail.com

[2]Technische Universität Berlin
Marchstrasse 12, Berlin 10587, Germany
flavio.silvestre@tu-berlin.de

Keywords: gain-scheduling, fuzzy logic, flexible aircraft, control design

Abstract: Previous works evidenced stability problems associated with flight control law design for flexible aircraft. In this paper, a fuzzy-based gain-scheduling approach is proposed to adequate closed-loop response. An interactive method that aims performance improvement while enforcing global stability considering fuzzy gain-scheduling was proposed. The application of the technique was demonstrated for the flexible X-HALE aircraft nonlinear model and compared to classical interpolation-based gain-scheduling techniques. Results revealed that fuzzy-based gain-scheduling is promising for flexible aircraft control.

1 INTRODUCTION

The interest in the class of unmanned vehicle known as High Altitude Long Endurance (HALE) aircraft has been growing in the latest years. An example is the Facebook HALE project Aquila designed to be hyper efficient, so it can fly for up to three months at a time [1]. Modern HALE aircraft designs have become so lightweight that increases flexibility, so traditional decoupled analyzes of flight mechanics and aeroelasticity are no longer adequate. The same trend can be observed for new-generation transport aircraft where aerodynamic efficiency results in wings of increasingly higher aspect-ratio [2, 3]. The increase in airframe flexibility of modern transport aircraft and high-altitude, long-endurance vehicles (HALE) imposes several challenges to flight control law design and implementation. These challenges are related to the progressive decrease of the frequencies that characterize the aeroelastic modes, the consequent coupling among the degrees of freedom of global motion (rigid-body modes) and the aeroelastic ones, and the continuous change in airframe configuration while the aircraft is deforming.

Various formulations that couple flight mechanics and aeroelastic dynamics have been proposed in last 40 years for different levels of airframe flexibility and model complexity [2–5]. The very-flexible experimental aircraft X-HALE has been proposed and build at the University of Michigan [6]. The aircraft, shown in figure 1, is currently in operation at ITA in Brazil as well.

The development of control systems for highly-flexible aircraft requires more complex models and control techniques than those adopted for slightly-flexible aircraft. Classically, control law

design is made assuming a rigid airframe, aeroelastic interaction effects are only considered a posteriori, typically through gain stabilization, using low-pass and notch filters [7]. However, this procedure can lead to a low-performance controller when the frequency ranges of flight and aeroelastic dynamics get tight to each other [3, 7]. Control law design based on flexible aircraft dynamics has been addressed by several authors in the literature [3, 7–11]. These approaches normally use structural state information as feedback signals in the control law. For simplicity, some of them still apply linear control theory.

A problem in controller synthesis using linear techniques is that the linearized model represents the dynamics only in a region close to the operation point, in some cases leading to system instability when the plant is subjected to variations, a common situation for very flexible aircraft. A wide range of linear control techniques can be employed to address this issue, such as robust control, that deal with systems uncertainty [12–14]. Nonlinear techniques can also be applied, such adaptive control, that proposes a predefined dynamics for the feedback gains that ensures stability and performance. These techniques often result in complex control laws hard to be implemented in practice [11, 15, 16]. For fixed-structure, linear-model-based controller, gain-scheduling is a good strategy, since it varies continuously the controller coefficients, calculated for various conditions, according to the current flight condition [17]. However classical gain-scheduling can cause abrupt changes in gains, which directly affect the dynamics of the plant, and may generate an undesirable performance [8]. Previous applications of fuzzy logic to gain-scheduling in flight control demonstrated the feasibility of this approach [18–21]. The fuzzy membership functions provide the interpolation of control parameters in a fuzzy-logic-based method, that allows an adjustment for a smoother variation of controller gains. Another advantage over the classical gain-scheduling is that closed-loop stability can be analytically guaranteed [22].

Taking advantage of the characteristic of fuzzy gain scheduling that allows global stability to be analytically guaranteed, an interactive method that combines performance and stability is proposed in this paper. The method is demonstrated for the flexible aircraft X-HALE to schedule the gains of its stability augmentation system (SAS), and compared to linear-interpolation- and nearest-based gain-scheduling approaches. The results reveal that the proposed method is promising for flexible aircraft control.

Figure 1: X-HALE aircraft with 4m wingspan that is currently in operation at ITA.

2 THEORETICAL DEVELOPMENT

2.1 Linear Control Law Design

2.1.1 The Inner-Loop: Stability Augmentation System

The plant can be naturally unstable due to many reasons, and when it happens a possible solution is to implement a SAS to improve the stability margins prior to designing the tracking loops.

To stabilize the plant and obtain an adequately-damped response a proportional output-feedback controller (block $\boldsymbol{K}$ in figure 2) is usually used in the inner-loop. The SAS gains were calculated using Linear Quadratic Regulator (LQR) technique by minimizing a performance index [8]. The minimization was accomplished numerically by a local search algorithm based on the Nelder-Mead simplex method.

2.1.2 The Outer-Loop: the Tracking System

The outer-loop has the structure of a traditional tracker. The tracking compensators were optimized through a non-smooth H_∞ synthesis [8]. In summary, the state-space system can be augmented by the compensator dynamics, which in closed-loop assumes the following form [23]:

$$\begin{aligned} \dot{\boldsymbol{x}}_{\boldsymbol{a}} &= \boldsymbol{A_c x_a} + \boldsymbol{B_c r} \\ \boldsymbol{y_a} &= \boldsymbol{C_a x_a} + \boldsymbol{F_a r} \\ \boldsymbol{z} &= \boldsymbol{H_a x_a} \\ \boldsymbol{u} &= \boldsymbol{K_a y_a} \end{aligned} \tag{1}$$

In Eq. 1 x_a is a vector containing the aircraft and compensator states, $\boldsymbol{y_a}$ is the augmented output vector considering measured variables of the aircraft dynamics and the output of the compensator, $\boldsymbol{z}$ is the vector of variables to be tracked, and $\boldsymbol{u}$ is the control vector. The gain matrix $\boldsymbol{K_a}$ includes the gain matrices of inner-loop $\boldsymbol{K}$ and outer-loop $\boldsymbol{L}$. The closed-loop state and control matrices are given by:

$$\begin{aligned} \boldsymbol{A_c} &= \boldsymbol{A_a} + \boldsymbol{B_a K_a C_a} \\ \boldsymbol{B_c} &= \boldsymbol{G_a} + \boldsymbol{B_a K_a F_a}. \end{aligned} \tag{2}$$

2.2 Gain-Scheduling

Linearized models cannot represent entire flight envelope due to large changes in the dynamic pressure during operation, which change considerably the dynamics of rigid body and aeroelastic. As a result, a constant linear model cannot be used to describe the entire flight envelope, and furthermore, traditional methods with a fixed gain set cannot fulfill the design requirements [17]. Gain-Scheduling, whose principle is adjusting the control law with the change of scheduled variable, is a control technique that enables the interpolation of control parameters between different design points to achieve satisfactory control tasks.

2.2.1 Classical Gain-Scheduling

The design of a gain-scheduled controller for a nonlinear plant can be described as a four-step procedure. The first step is to compute a linearization of the nonlinear plant in the desired equilibrium points, also called operating points or set points. The second step is the use linear design methods to design linear controllers for each linear model obtained in previous step, in order to achieve the requirements for each equilibrium condition. The third step consists in

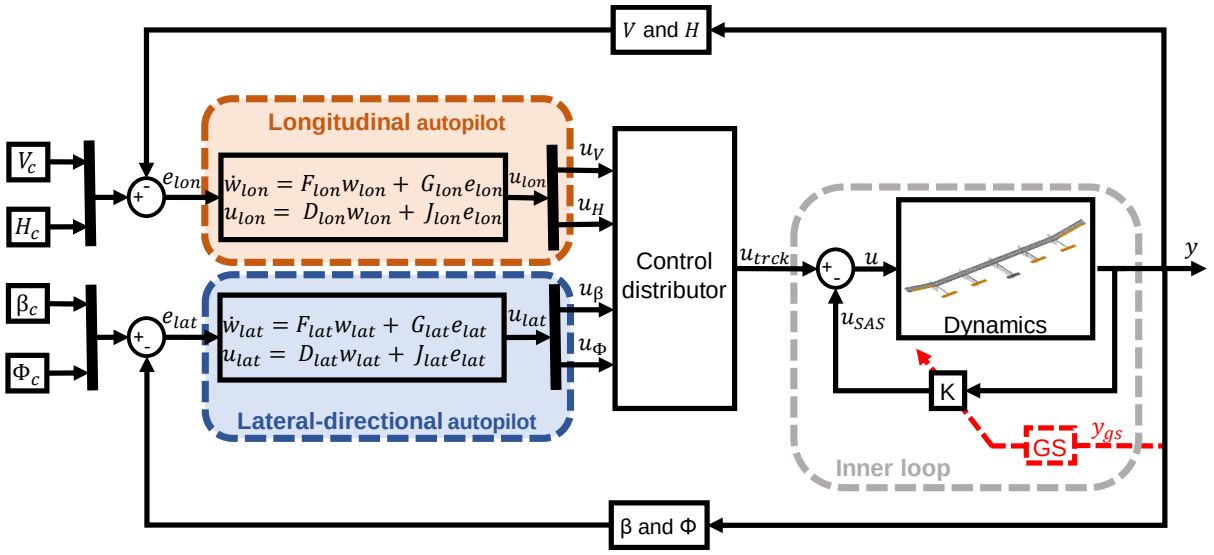

Figure 2: Block diagram of a flight control system

implementing the family of linear controllers such that the controller coefficients (gains) are varied (scheduled) according to the current value of the scheduled variables [17], represented in figure 2 by "GS". Finally, the fourth step is performance and stability. Typically, stability can be assured only locally and in a slow-variation setting, but it is by far not guaranteed. The same applies to control performance. Depending on the scheduling strategy, performance may fall drastically [8]. Normally, stability and performance must be assessed based on simulation studies [17]. Depending on the number of parameters that may vary and change the plant, the number of simulations to be performed may increase drastically, resulting in a very costly control law development process.

2.2.2 Fuzzy-logic-based Gain-Scheduling (FGS)

The fuzzy-logic is based on "IF antecedent THEN consequence" rules, called heuristic rules, and any rule is composed of an antecedent and a consequence, where both can receive more than one preposition. Among the fuzzy logic classes, the Takagi-Sugeno (TS) one has the particularity of containing a linear input-output relation in the consequence [24].

The FGS controller is a TS-type fuzzy controller and follows the same steps as the classical gain-scheduling. However, it employs a different interpolation strategy, which enables a stability analysis of the *fuzzified* model [22].

At each design point $y_{gs_i}(i = 1, 2, \ldots, l)$, with l design variable points, the system described in Eq. (1) is approximated by the fuzzy rule was follow:

$$R_i: \quad \text{If} \quad y \quad \text{is} \quad y_{gs_i} \quad \text{then} \quad \dot{\boldsymbol{x}} = \boldsymbol{A}_i\boldsymbol{x} + \boldsymbol{B}_i\boldsymbol{u} \quad \text{and} \quad \boldsymbol{y} = \boldsymbol{C}_i\boldsymbol{x} + \boldsymbol{D}_i\boldsymbol{u} \tag{3}$$

where R_i is the i^{th} rule, y_{gs_i} is the fuzzy set for each rule, "y is y_{gs_i}" is the antecedent (given that y is the crisp value of the scheduled variable) and "$\dot{\boldsymbol{x}} = \boldsymbol{A}_i\boldsymbol{x} + \boldsymbol{B}_i\boldsymbol{u}$ and $\boldsymbol{y} = \boldsymbol{C}_i\boldsymbol{x} + \boldsymbol{D}_i\boldsymbol{u}$" is the consequence, with two linear input-output relations. The control law is defined by:

$$R_i: \quad \text{If} \quad y \quad \text{is} \quad y_{gs_i} \quad \text{then} \quad \boldsymbol{u} = \boldsymbol{K}_i\boldsymbol{y} \tag{4}$$

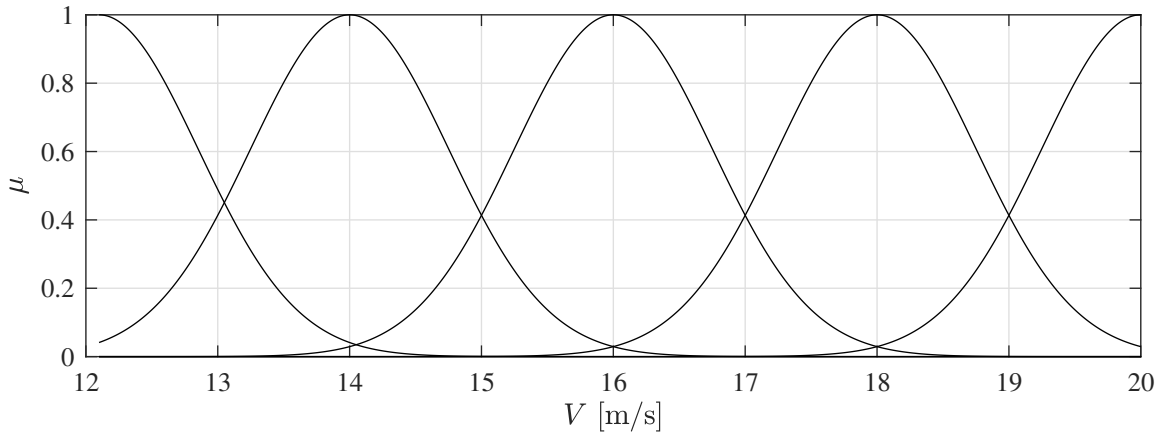

Figure 3: Designed membership functions

The membership functions used to interpolate the rules have many different forms (triangular, trapezoidal, bell, Gaussian, etc). We consider herein the Gaussian form, which has its weights given by:

$$\mu_i(v) = exp(-(\frac{y - y_{gs_i}}{2\sigma})^2) \tag{5}$$

The weight is the mathematical form to ponder each rule, according to the value of scheduled variable, and σ (standard deviation) is a project parameter that measures how the neighbor antecedents affect the actual consequence. In figure 3 five membership functions (μ) with Gaussian form are displayed, and the weight for each rule is given by μ. Eventually, the weights are normalized by the sum of all rules weights, so that the sum of all normalized weights is always equal to 1. Therefore, the normalized weights ω_i are given by:

$$\omega_i = \frac{\mu_i}{\sum_{i=1}^{l} \mu_i} \tag{6}$$

The system can now be represented by:

$$\dot{\boldsymbol{x}} = \sum_{i=1}^{l} \omega^i(\boldsymbol{A}_i\boldsymbol{x} + \boldsymbol{B}_i\boldsymbol{u}), \tag{7}$$

$$\boldsymbol{y} = \sum_{i=1}^{l} \omega^i(\boldsymbol{C}_i\boldsymbol{x} + \boldsymbol{D}_i\boldsymbol{u}), \tag{8}$$

and the control law by:

$$\boldsymbol{u} = \sum_{i=1}^{l} \omega^i(\boldsymbol{K}_i\boldsymbol{y}). \tag{9}$$

The effectiveness of the FGS controller relies on tuning of both the LQR controllers and σ. The LQR parameter affects the performance and stability at each design project point, and the σ tune how smooth the transition between these points will be.

3 FLIGHT CONTROL LAW DESIGN FOR A VERY FLEXIBLE AIRCRAFT

3.1 Model Description

In this paper, the VFA X-HALE was considered. The X-HALE, Fig 4, is a high-aspect-ratio aircraft, with a wingspan of $6m$ and a chord of $0.2m$, whose wing is formed by six panels of 1m each one. The two outer panels of the wing have a dihedral angle of 10 degrees and each one has one aileron. The aircraft has five equidistant fuselages mounted under the wing to accommodate electric motors and instrumentation. Five horizontal stabilizers. The central one is only used in a flipping mode to increase the directional stability of the aircraft when in vertical tail configuration, thus reducing the pilot workload. The two outer horizontal stabilizers (elevons) of each side are used for active control and can be deflected in any possible combination. The central and two inner booms have ventral fins for improvement of the lateral-directional stability [6, 13]. Figure 4 shows the aircraft's geometry and the control inputs are indicated with the corresponding nomenclature. Velocity flight envelope is limited between 12 and $20m/s$.

The flight dynamics has been modeled according the formulation presented by Guimares Neto et al. [3], applicable to moderately flexible aircraft. Basically, the model is composed by the classical rigid-body equations of motion coupled with structural dynamics characterized by a finite-element representation, assuming small elastic deformations. The incremental unsteady aerodynamics is modeled using the Doublet-Lattice Method [25] with rational function approximations [26] and appropriate aerodynamic influence coefficient corrections to take viscous effects into account.

The model describes the dynamic equations of motion in the inertial reference frame, for all six degrees of freedom: displacements in the x and y directions, altitude H and roll, pitch and yaw angles (ϕ, θ and ψ, respectively). Furthermore, the velocity V, the angle of attack α, the sideslip angle β, as well as the angular rates p, q and r are also described. A particular

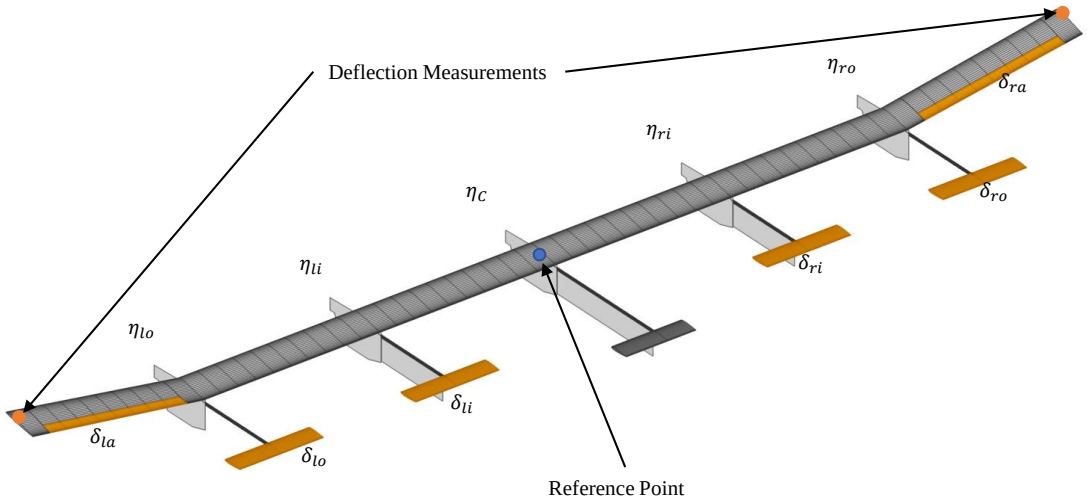

Figure 4: X-HALE aircraft.

feature of the model is the representation of structural dynamics using modal amplitudes and their time-derivatives ($\boldsymbol{\eta}$ and $\dot{\boldsymbol{\eta}}$). Aerodynamic lag states arise due to rigid-body and control surfaces dynamics ($\boldsymbol{\lambda_{rb}}$) and to the aeroelastic dynamics ($\boldsymbol{\lambda_{\eta}}$). The state vector $\boldsymbol{x}$ is:

$$\boldsymbol{x} = \left[\boldsymbol{x_{rb}}^T,\, \boldsymbol{\lambda_{rb_{84\times 1}}}^T,\, \boldsymbol{\eta_{14\times 1}}^T,\, \dot{\boldsymbol{\eta}}_{\mathbf{14\times 1}}^T,\, \boldsymbol{\lambda_{\eta_{98\times 1}}}^T\right]^T \tag{10}$$

Six control surfaces, including four elevons (δ_{ro}, δ_{ri}, δ_{li}, δ_{lo}) and two ailerons (δ_{ra}, δ_{la}), and five motors (η_{ro}, η_{ri}, η_c, η_{li}, η_{lo}) give the control input of the X-HALE, as seen in figure 4. The system contains a total of 11 inputs:

$$\boldsymbol{u} = \left[\delta_{li},\, \delta_{ri},\, \delta_{lo},\, \delta_{ro},\, \delta_{la},\, \delta_{ra},\, \eta_{lo},\, \eta_{li},\, \eta_c,\, \eta_{ri},\, \eta_{ro}\right]^T \tag{11}$$

where the subscript l means left side of the aircraft, r right side, o outer, i inner and c central position. The 116 outputs comprise measurements such as displacements and attitude, linear and angular velocities, load factors, at different points of the wing, stabilizers and pods. In addition, it is also possible to recover structural displacements and twists.

3.2 Linear Control Law Design

The SAS was designed based on the loop-separation approach. It is able to stabilize the plant while it regulates rigid body motions and control the shape of one-half wing independently from the other [10]. To achieve these goals a proportional output-feedback controller was designed with the angular rates p, q, r, pitch attitude (θ) and roll angle (ϕ) for stabilization and the elastic vertical translations of the reference points (T) on the tip of the wings shown in figure 4 for shape control. Pitch attitude and angular rate q is controlled by the inner elevons (δ_{li} and δ_{ri}), operating symmetrically, while roll angle and angular rates p and r is controlled by the outer elevons (δ_{lo} and δ_{ro}), operating antisymmetrically. Ailerons (δ_{la} and δ_{ra}) is employed for shape control, where the sum of the structural displacements of the wing tips is fed back to the ailerons symmetrically to deal with symmetrical wing bending modes, while the difference is fed back to the ailerons anti-symmetrically to deal with anti-symmetrical wing bending modes, as described bellow:

$$\begin{bmatrix}\delta_{la}\\ \delta_{ra}\end{bmatrix} = \begin{bmatrix}K_6 & K_7\\ K_6 & K_7\end{bmatrix} * \begin{bmatrix}T_{zl}\\ T_{zr}\end{bmatrix} + \begin{bmatrix}-K_8 & K_9\\ K_8 & -K_9\end{bmatrix} * \begin{bmatrix}T_{zl}\\ T_{zr}\end{bmatrix} \tag{12}$$

Motors were not used in the SAS. The final form of the gain matrix $\boldsymbol{K}$ is:

$$\begin{bmatrix}\delta_{li}\\ \delta_{ri}\\ \delta_{lo}\\ \delta_{ro}\\ \delta_{la}\\ \delta_{ra}\end{bmatrix} = \underbrace{\begin{bmatrix}K_1 & K_2 & 0 & 0 & 0 & 0 & 0\\ K_1 & K_2 & 0 & 0 & 0 & 0 & 0\\ 0 & 0 & -K_3 & -K_4 & -K_5 & 0 & 0\\ 0 & 0 & K_3 & K_4 & K_5 & 0 & 0\\ 0 & 0 & 0 & 0 & 0 & K_6-K_8 & K_7+K_9\\ 0 & 0 & 0 & 0 & 0 & K_6+K_8 & K_7-K_9\end{bmatrix}}_{\boldsymbol{K_{sas}}} \begin{bmatrix}\theta\\ q\\ \phi\\ p\\ r\\ T_{zl}\\ T_{zr}\end{bmatrix} \tag{13}$$

The compensator was designed separately, the longitudinal part tracking velocity (V) and altitude (H) while the lateral-directional part is responsible to track sideslip angle (β) and roll angle (ϕ). The control distributor block seen in Fig. 2 is a boolean matrix with the function of selecting which aircraft control input will be employed to track each variable of interest. The first two compensator outputs, referring to V and H, will be controlled by the inner elevons (δ_{li}

and δ_{ri}), operating symmetrically, as well the motors (η_{lo}, η_{li}, η_c, η_{ri} and η_{ro}), also operating in a symmetric way. The second two compensator outputs, referring to β and ϕ, will be controlled by the outer motors (η_{lo}, η_{li}, η_{ri} and η_{ro}) and outer elevons (δ_{lo} and δ_{ro}) respectively, both operating anti-symmetrically.

3.3 Motivation

3.3.1 Static gain

When linear techniques are used to design a control law for a plant that may vary significantly within the range of operation, instabilities may occur. The control law designed for the flexible aircraft X-HALE, a SAS coupled with a robust linear controller to track velocity, altitude, sideslip and roll angle, highlighted this problem when it failed to ensure stability for a variation of $4m/s$ in a coordinate turn, as shown in the figure 5, due to nonlinearities present in the plant [8]. Nonlinear simulation results have shown that after the velocity of $18m/s$ is reached, the roll rate p gets unstable.

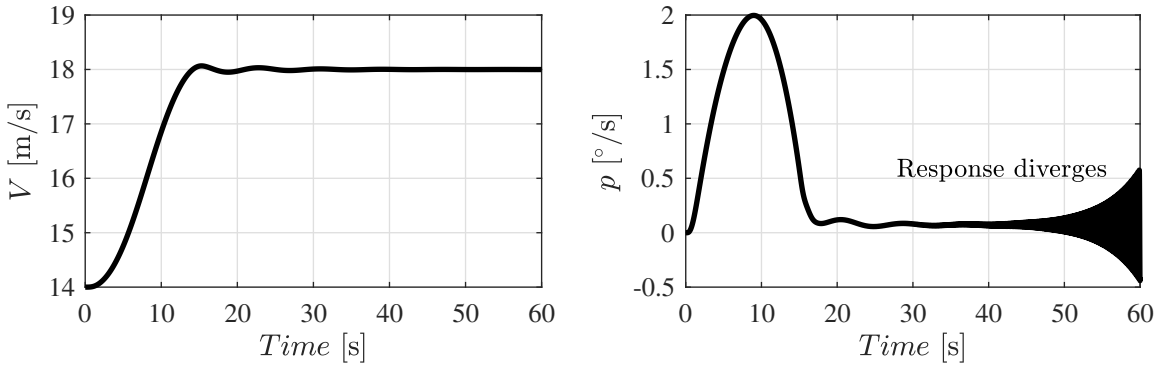

Figure 5: Roll instability in a coordinated turn for a variation of $4m/s$ in the flight velocity.

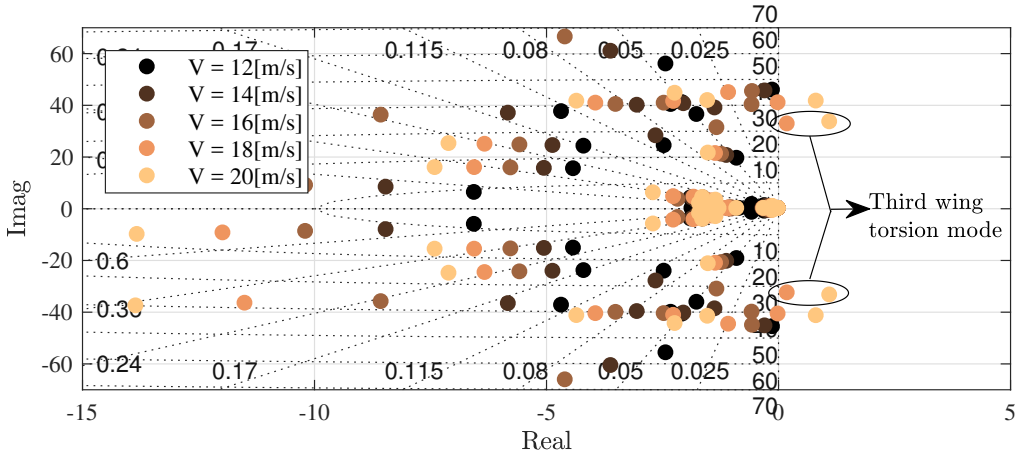

Figure 6: Root-loci of closed loop system for increasing velocity.

In the case shown above, the SAS was designed for a model linearized at $14m/s$. We observe at the figure 6 that the poles related to the third wing torsion mode in closed-loop go towards the right side of the complex plane with a velocity increase.

3.3.2 Scheduled gain

In an attempt to overcome the problem demonstrated in the previous case, with a static gain, a gain-scheduling was designed. The model was linearized in five operation points (12 to $20m/s$, with $2m/s$ of step), and for each point a SAS was calculated. Observing the closed-loop root-loci with gain-scheduling for the SAS, see figure 7, shows that the technique was able to move all poles to the left side of the complex plane. The root-loci were generated considering only the closed-loop poles at the given edge velocity, i.e. in terms of stability nothing can be said a priori in the continuous velocity range, between the edge velocities.

Nonlinear simulations using the model described in section 3.1 were performed to validate the efficiency of the two gain-scheduling techniques: a linear interpolation between the gains; and

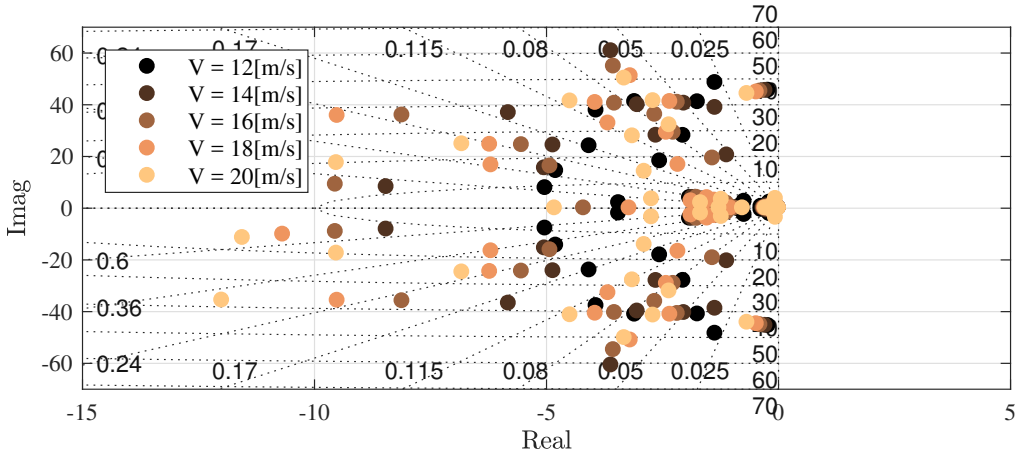

Figure 7: Root-loci of closed loop system for increasing velocity with fuzzy gain-scheduling in inner-loop.

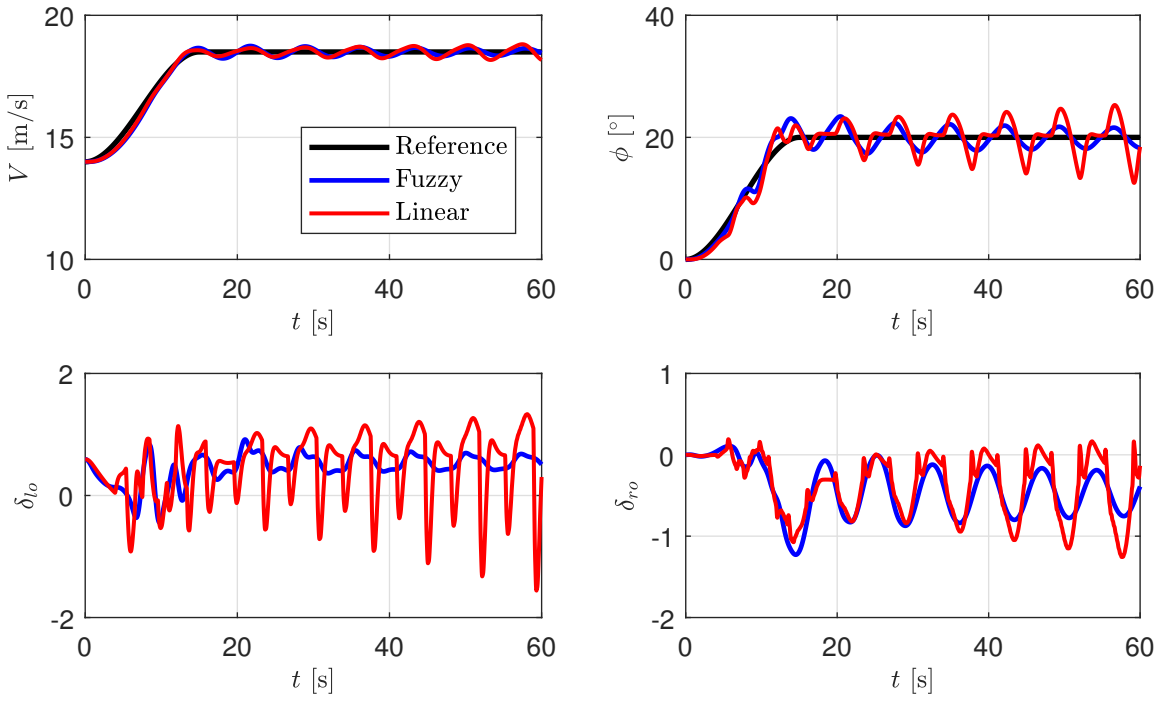

Figure 8: Measurements and Controls for a variation of 4.5m/s in a coordinated turn with nonlinear model.

the fuzzy technique, explained in previous section. A maneuver was simulated, considering an increase of $4.5m/s$ in the reference velocity to be tracked, while the reference for roll angle was $20deg$; altitude and sideslip angle were regulated to zero. Tracking references are smooth ramps of 15 seconds settling time [21].

The results show a slow divergence considering the linear gain-scheduling and a slow convergence considering the fuzzy one when the velocity reaches a value close to $18.5m/s$, Fig. 8. Even if the response considering fuzzy gain-scheduling is stable, the stability is marginal and the low oscillation damping is not acceptable.

Once the results was unsatisfactory, a new design method is proposed to find the scheduled gains, taking advantage of the characteristic of fuzzy gain scheduling that allows global stability to be analytically guaranteed.

4 FUZZY GAIN-SCHEDULING WITH PERFORMANCE CONCERN AND STABILITY ENFORCEMENT

The Lyapunov direct method [27] can be employed to verify the system stability within the range of operation. This method seeks to determine the parameters of a Lyapunov function, belonging to a particular candidate class, that guarantee the stability of the investigated system. Consider a Lyapunov candidate in quadratic form, for a given positive definite matrix P to be determined:

$$V = \boldsymbol{x}^T \boldsymbol{P} \boldsymbol{x} \tag{14}$$

For the open-loop system described in equation 7, the derivative of the Lyapunov candidate function will be

$$\begin{aligned} \dot{V} &= \dot{\boldsymbol{x}}^T \boldsymbol{P} \boldsymbol{x} + \boldsymbol{x}^T \boldsymbol{P} \dot{\boldsymbol{x}} && (15)\\ &= \boldsymbol{x}^T \boldsymbol{A}(\omega)^T \boldsymbol{P} \boldsymbol{x} + \boldsymbol{x}^T \boldsymbol{P} \boldsymbol{A}(\omega) \boldsymbol{x} && (16)\\ &= \boldsymbol{x}^T [\boldsymbol{A}(\omega)^T \boldsymbol{P} + \boldsymbol{P} \boldsymbol{A}(\omega)] \boldsymbol{x} && (17)\\ &= \boldsymbol{x}^T \sum_{i=1}^{l} \omega_i [\boldsymbol{A}_i^T \boldsymbol{P} + \boldsymbol{P} \boldsymbol{A}_i] \boldsymbol{x}. && (18) \end{aligned}$$

The stability of the system can be guaranteed if $\dot{V} < 0$ for all possible states x [27]. Since the sum $\sum_{i=1}^{l} \omega$ is always equal to one (eq. 6), a sufficient condition for stability is given by Theorem 1 below, that imposes a set of linear matrix inequalities (LMI) to be concomitantly solved for P.

Theorem 1 *[28]. The system represented in equation 7 is asymptotically stable if there is a positive definite matrix* $\boldsymbol{P}$ *that satisfy*

$$\boldsymbol{A}_i^T \boldsymbol{P} + \boldsymbol{P} \boldsymbol{A}_i < 0, i = 1, 2, \ldots, l. \tag{19}$$

In order to evaluate a closed-loop system stability, a substitution can be made in the system presented in equation 19 by changing $\boldsymbol{A}_i$ by $\boldsymbol{A}_{ci}$, where $\boldsymbol{A}_{ci}$ is the closed-loop system defined as $\boldsymbol{A}_{ci} = \boldsymbol{A}_i + \boldsymbol{B}_i \boldsymbol{K}_i$ for state feedback or $\boldsymbol{A}_{ci} = \boldsymbol{A}_i + \boldsymbol{B}_i \boldsymbol{K}_i \boldsymbol{C}_i$ for output feedback.

Applying Theorem 1 to the gains found in the previous section using the Cholesky-based linear algebra solver [29] through MATLAB software, a feasible solution can not be found. There are less conservative ways of analyzing a TS system when compared to the quadratic stability presented in Theorem 1, which takes into account only the polytopic characteristics of the system. Mozelli [30] proposes some ways of reducing conservatism through the use of the rate of temporal variation of membership functions in the formulation. However, this addition eventually increases the complexity of the LMIs, making the computational process more costly, which is already a limiting factor in the case of high order systems. Table 1 shows a comparison between Theorem 1 and Mozellis alternative [30].

Table 1: Complexity analysis for LMI conditions based on the quadratic and fuzzy Lyapunov functions: L number of lines, V number of variables, n system order, r number of rules.

Method	L	V
Theorem 1	$n(r+1)$	$0.5(n^2+n)$
Fuzzy Lyapunov	$0.5n(r^2+5r)$	$0.5(n^2+n)(r+1)$

It is possible to expand the stability analysis in order to insert the controller gains as variables. So the controller gains will be inserted into the derivative of the Lyapunov function of equation 16, resulting in:

$$\dot{V} = \boldsymbol{x}^T[\boldsymbol{A}(\omega) + \boldsymbol{B}(\omega)\boldsymbol{K}(\omega)]^T\boldsymbol{P}\boldsymbol{x} + \boldsymbol{x}^T\boldsymbol{P}[\boldsymbol{A}(\omega) + \boldsymbol{B}(\omega)\boldsymbol{K}(\omega)]\boldsymbol{x} \tag{20}$$

$$= \boldsymbol{x}^T([\boldsymbol{A}(\omega) + \boldsymbol{B}(\omega)\boldsymbol{K}(\omega)]^T\boldsymbol{P} + \boldsymbol{P}[\boldsymbol{A}(\omega) + \boldsymbol{B}(\omega)\boldsymbol{K}(\omega)])\boldsymbol{x}. \tag{21}$$

Therefore, it is enough to ensure

$$[\boldsymbol{A}(\omega) + \boldsymbol{B}(\omega)\boldsymbol{K}(\omega)]^T\boldsymbol{P} + \boldsymbol{P}[\boldsymbol{A}(\omega) + \boldsymbol{B}(\omega)\boldsymbol{K}(\omega)] < 0. \tag{22}$$

At this point it is noted that the inequality is not a LMI, since there are two sets of matrix variables to be determined that are multiplied: one being the gain matrix $\boldsymbol{K}(\omega)$ and the other being the Lyapunov matrix $\boldsymbol{P}$. The simplicity by which such inequalities can be converted into LMIs is the great attraction of quadratic stability criterion. Using the transformations $\boldsymbol{W} = \boldsymbol{P}^{-1}$ and $\boldsymbol{Z}(\omega) = \boldsymbol{K}(\omega)\boldsymbol{W}$ we obtain the equivalent condition

$$\boldsymbol{W}\boldsymbol{A}(\omega)^T + \boldsymbol{A}(\omega)\boldsymbol{W} + \boldsymbol{Z}(\omega)^T\boldsymbol{B}(\omega)^T + \boldsymbol{B}(\omega)\boldsymbol{Z}(\omega) < 0 \tag{23}$$

$$\sum_{i=1}^{l} \omega_i(\boldsymbol{W}\boldsymbol{A}_i^T + \boldsymbol{A}_i\boldsymbol{W} + \boldsymbol{Z}_i^T\boldsymbol{B}_i^T + \boldsymbol{B}_i\boldsymbol{Z}_i) < 0 \tag{24}$$

A linear set of inequalities in the $\boldsymbol{W}$ and $\boldsymbol{Z}_i$ variables is now available. For simplicity, it was considered that the membership functions for the system and for the control are exactly the same, reducing the amount of inequalities that must be solved. Thus we achieve the following theorem.

Theorem 2 *[28]. The system represented in equation 7 is asymptotically stable if there is a positive definite matrix $\boldsymbol{W}$ and any matrices $\boldsymbol{Z}_i$ that satisfy*

$$\boldsymbol{W}\boldsymbol{A}_i^T + \boldsymbol{A}_i\boldsymbol{W} + \boldsymbol{Z}_i^T\boldsymbol{B}_i^T + \boldsymbol{B}_i\boldsymbol{Z}_i < 0, i = 1, 2, \ldots, l. \tag{25}$$

If there is a feasible solution to the inequalities presented in Theorem 2, the gains of the stabilizing controller can be obtained by solving $\boldsymbol{K}_i = \boldsymbol{Z}_i \boldsymbol{W}^{-1}$, and the Lyapunov function that guarantees closed-loop stability, obtained from the inverse of $\boldsymbol{W}$.

Despite the global stability, this method does not introduce any performance requirement. The resulting gains will most likely present an inadequate response. In this sense, studies [31, 32] have been carried out with the intention of inserting performance criteria in the solution of these equations, unfortunately resulting in an increase of the computational cost of the method.

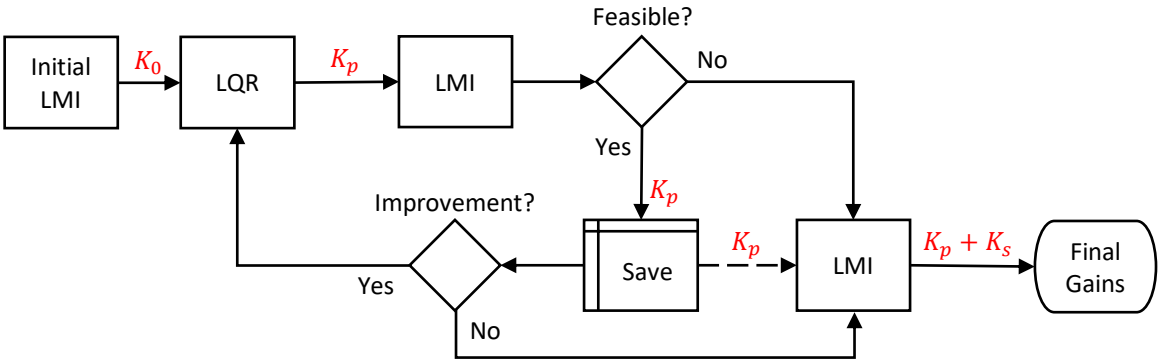

Figure 9: Flowchart of the interactive optimization process of FGS.

With the idea of combining the simplicity of Theorem 2, especially with regard to computational cost, and a focus on performance improvement, an interactive methodology for designing a fuzzy gain-scheduling controller was proposed following the steps shown in the flowchart in Fig. 9:

1. The first step ("Initial LMI") is the application of Theorem 2 in the open-loop system, in order to obtain the initial gains ($\boldsymbol{K}_0$) for the linear control technique;
2. the initial gains found in the previous step ($\boldsymbol{K}_0$) are used for evaluation of the LQR, resulting the gain matrix ($\boldsymbol{K}_p$) optimized according to that described in section 2.1.1, for all design points;
3. test if there exist a set of gains ($\boldsymbol{K}_s$) such that $\boldsymbol{K}_p + \boldsymbol{K}_s$ stabilize the closed-loop system, using the gains ($\boldsymbol{K}_p$) found in optimization, by means of Theorem 2;
4. in case that the test was feasible, save the gains ($\boldsymbol{K}_p$); otherwise, go to step 6;
5. if there is a significant improvement in the LQR performance index with the new gain

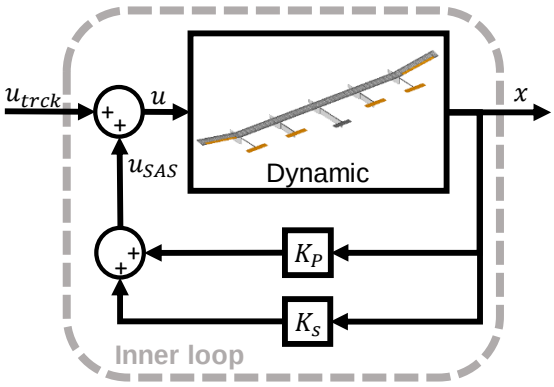

Figure 10: Inner loop with the two proposed gains.

matrix ($\boldsymbol{K}_p$), return to the optimization through the LQR using the current $\boldsymbol{K}_p$ as initial gains ($\boldsymbol{K}_0$), step 2, otherwise, go to next step;

6. $\boldsymbol{K}_s$ is than calculated according to Theorem 2, so that $\boldsymbol{K}_p + \boldsymbol{K}_s$ stabilize the closed loop system; $\boldsymbol{K}_p + \boldsymbol{K}_s$ is than the final gain matrix.

4.1 Model Reduction

The high order of the X-HALE model is a challenge to most of the control techniques and therefore a state-space reduced-order model is appropriate. For this purpose, a residualization technique is applied to all the aerodynamic lag states of the nominal model [33]. The resulting reduced linear model ($\boldsymbol{A_p}$, $\boldsymbol{B_p}$, $\boldsymbol{C_p}$, $\boldsymbol{D_p}$) comprises nine rigid-body states of the full model (discarding ignorable variables x, y and ψ) as well as the aeroelastic ones:

$$\boldsymbol{x_p} = \left[\begin{array}{cccccccccc} V & \alpha & q & \theta & H & \beta & \phi & p & r & \boldsymbol{\eta}^T \quad \dot{\boldsymbol{\eta}}^T \end{array} \right]^T \tag{26}$$

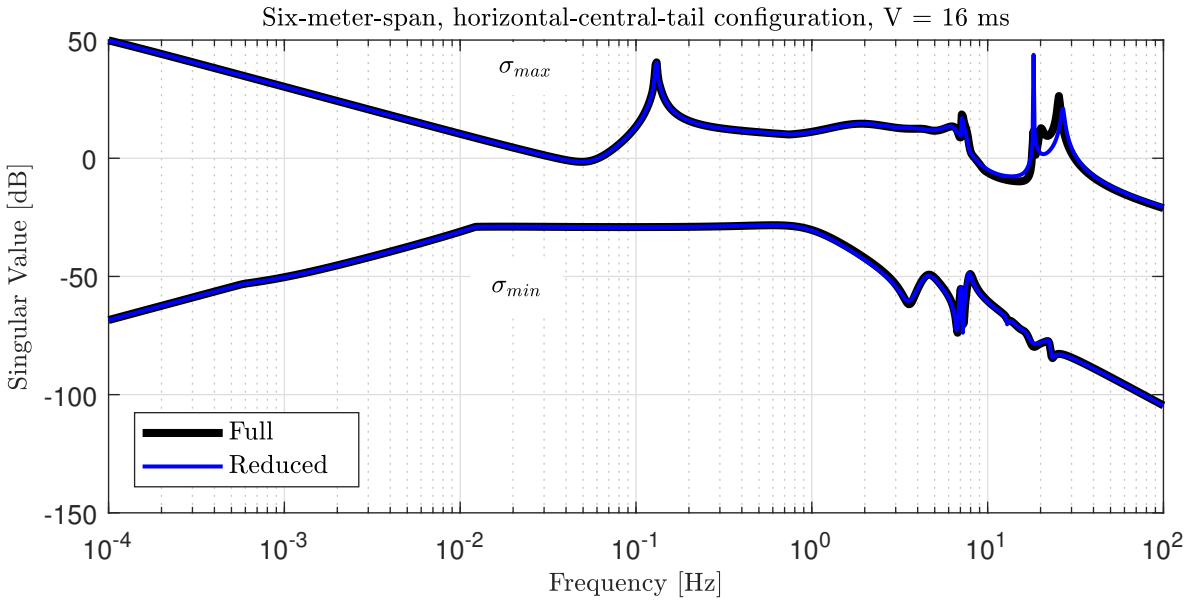

Figure 11: Comparison between the maximum and minimum singular values of the transfer function matrices for both full and reduced models.

The maximum and minimum singular values of the MIMO transfer function matrix for both full and reduced models is showed in Fig. 11. It is notorious that the reduced model preserves sufficient characteristics of the full one.

4.2 Results

To exemplify the proposed method, the technique described in the previous section was applied to the reduced order model of the six-meter-span X-HALE configuration, described in section 4.1.

All aircraft actuators (Eq. (11)) can be independently commanded. However to reduce the number of gains to be determined, and assuming that the aircraft is nearly symmetric in the xz plane, a couple of command rules mixing the actuators are enforced. In this philosophy, it was defined that the inner elevons δ_{li} and δ_{ri} operate symmetrically as elevators ($\delta_{li} = \delta_{ri}$) and the outer elevons δ_{lo} and δ_{ro} operate anti-symmetrically like ailerons ($\delta_{li} = -\delta_{ri}$). The outer electric motors are used differentially to generate yawing motion ($\eta_C - (\eta_{lo} + \eta_{li}) = (\eta_{ro} + \eta_{ri}) - \eta_C$),

in substitution of a rudder, while all motors operate together to generate thrust - in this case, the total thrust is the sum of all motors ($\eta_C + \eta_{lo} + \eta_{li} + \eta_{ro} + \eta_{ri}$). Finally the ailerons δ_{la} and δ_{ra} were left free and are intended to correct the shape of the aircraft. Then the input vector can be rewritten as:

$$\boldsymbol{u} = [\delta_e \quad \delta_a \quad \delta_{ra} \quad \delta_{la} \quad \delta_t \quad \delta_r]^T \tag{27}$$

where $\boldsymbol{u} \in \mathbb{R}^{6\times 1}$. The previous assumptions are mathematically represented by the following restructuring of output matrix for disturbances around equilibrium:

$$\boldsymbol{B_\delta} = \left[\boldsymbol{B_1} + \boldsymbol{B_2} \;\vdots\; \boldsymbol{B_4} - \boldsymbol{B_3} \;\vdots\; \boldsymbol{B_7} + \boldsymbol{B_8} + \boldsymbol{B_9} + \boldsymbol{B_{10}} + \boldsymbol{B_{11}} \;\vdots\; (\boldsymbol{B_{10}} + \boldsymbol{B_{11}}) - (\boldsymbol{B_7} + \boldsymbol{B_8})\right] \tag{28}$$

where $\boldsymbol{B_j}$ represents the j-th column of the matrix $\boldsymbol{B}$, $\boldsymbol{B_\delta} \in \mathbb{R}^{n\times 6}$. Altitude state was disregarded for the calculation of the inner loop, and the linear model employed in the SAS design reads:

$$\dot{\boldsymbol{x}} \;=\; \boldsymbol{A_{36\times 36}}\boldsymbol{x} + \boldsymbol{B_{\delta_{36\times 6}}}\boldsymbol{u} \tag{29}$$

After this simplification in matrix $\boldsymbol{B}$, the gains were developed according to the methodology of the flowchart of Fig. 9, a good compromise between closed-loop response and demanded actuation energy was obtained for the following choice of weighting matrices:

$$\begin{aligned} \boldsymbol{Q} &= \begin{bmatrix} \boldsymbol{I}_{8\times 8} & \boldsymbol{0}_{8\times 28} \\ \boldsymbol{0}_{28\times 8} & 10^{-3}\boldsymbol{I}_{28\times 28} \end{bmatrix} \\ \boldsymbol{R} &= 10^3 \boldsymbol{I}_{6\times 6} \end{aligned} \tag{30}$$

and the number of steps to optimize the gains in LQR sense was 28800. For fuzzy scheduling, the same membership functions of Fig. 3 were used, with $\sigma = 0.75$. The tracking outer loop was designed in the same way described in section 2.1.2.

In order to verify the difference between the gain before the inclusion of the stabilizing gain ($\boldsymbol{K_s}$) and after the inclusion ($\boldsymbol{K}_p + \boldsymbol{K}_s$), the relation between the performance index is calculated for each flight velocity and it is shown in table 2.

Table 2: Comparison of the performance index with and without the stabilizing gain ($\boldsymbol{K_s}$).

Velocity [m/s]	$J(K_p + K_s)/J(K_p)$
12	15.78
14	2.88
16	1.76
18	1.78
20	1.71

As expected, there was an increase in performance index value, which apparently indicates a degradation in the performance when the stabilization part of the gain is added. To analyze the degradation in the closed loop performance, a turning maneuver tracking 20 degrees of roll angle, while decreasing the velocity by 5 meters per second, starting at an initial velocity condition of $14m/s$, was performed in the *fuzzified* plant. The commanded references for roll angle and velocity are smooth ramps of 1.33 degrees per second and 0.13 meters per second, respectively, until the full reference value is reached.

The results of Figures. 12 and 13, show that when the velocity comes close to $19m/s$, about 35 seconds in simulation time, the feedback regarding performance only (without stability constraints) begins to oscillate in a divergent way, since the system reach an unstable region in the envelope with the velocity increase. On the other hand, the controller that takes into account the global stability had a good tracking performance, with small oscillations in velocity and altitude and practically without oscillations in roll and slide-slip angles. It is also important to notice that the control actuators remained well below the physical limits of the aircraft.

Stability margins of the MIMO system have been calculated according to Ref. [34] for the two cases of feedback: that with the performance gain only, and the one arising from the superposition of a stabilizing gain according to the flowchart of Fig. 9. The resulting stability margins can be seen in Fig. 14, where one can observe that the proposed methodology results in better behaved margins throughout the velocity envelope, while the performance optimization results in low stability margins, and even in instability for a couple of points in the velocity envelope.

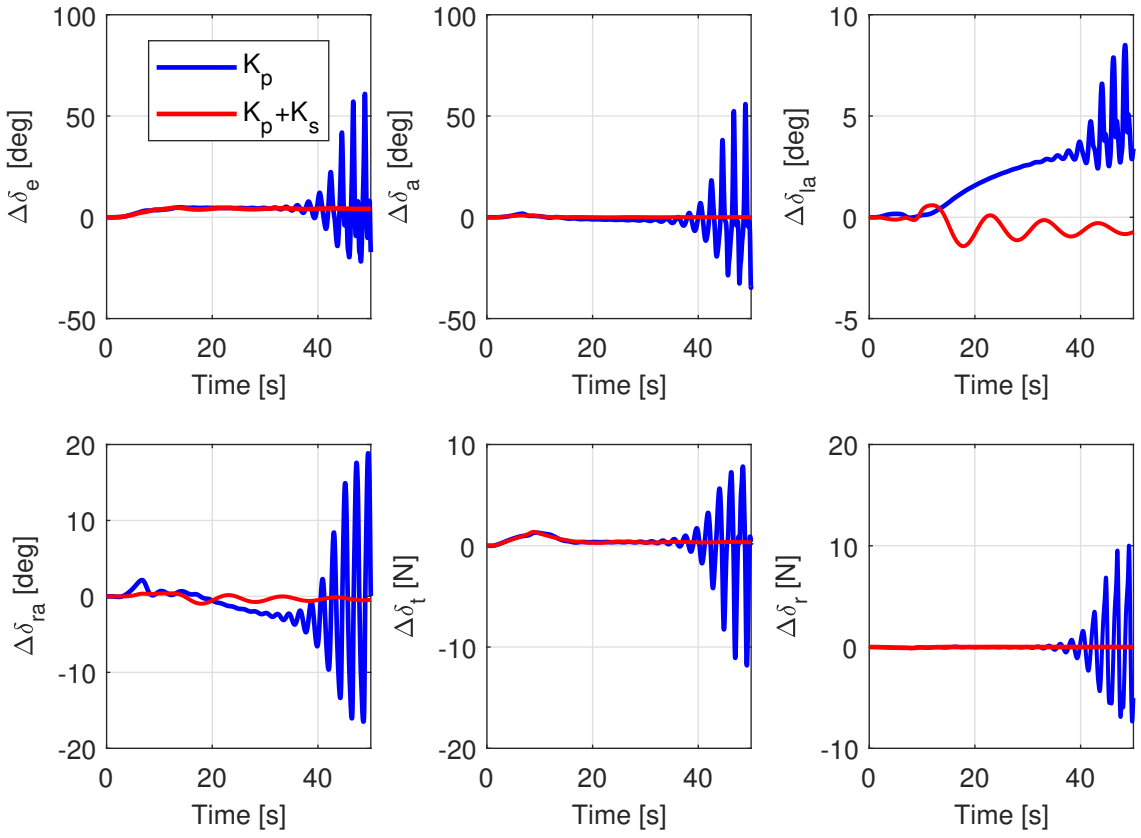

Figure 12: Control commands for a variation of 5m/s in a coordinated turn with fuzzy interpolation state-space matrices.

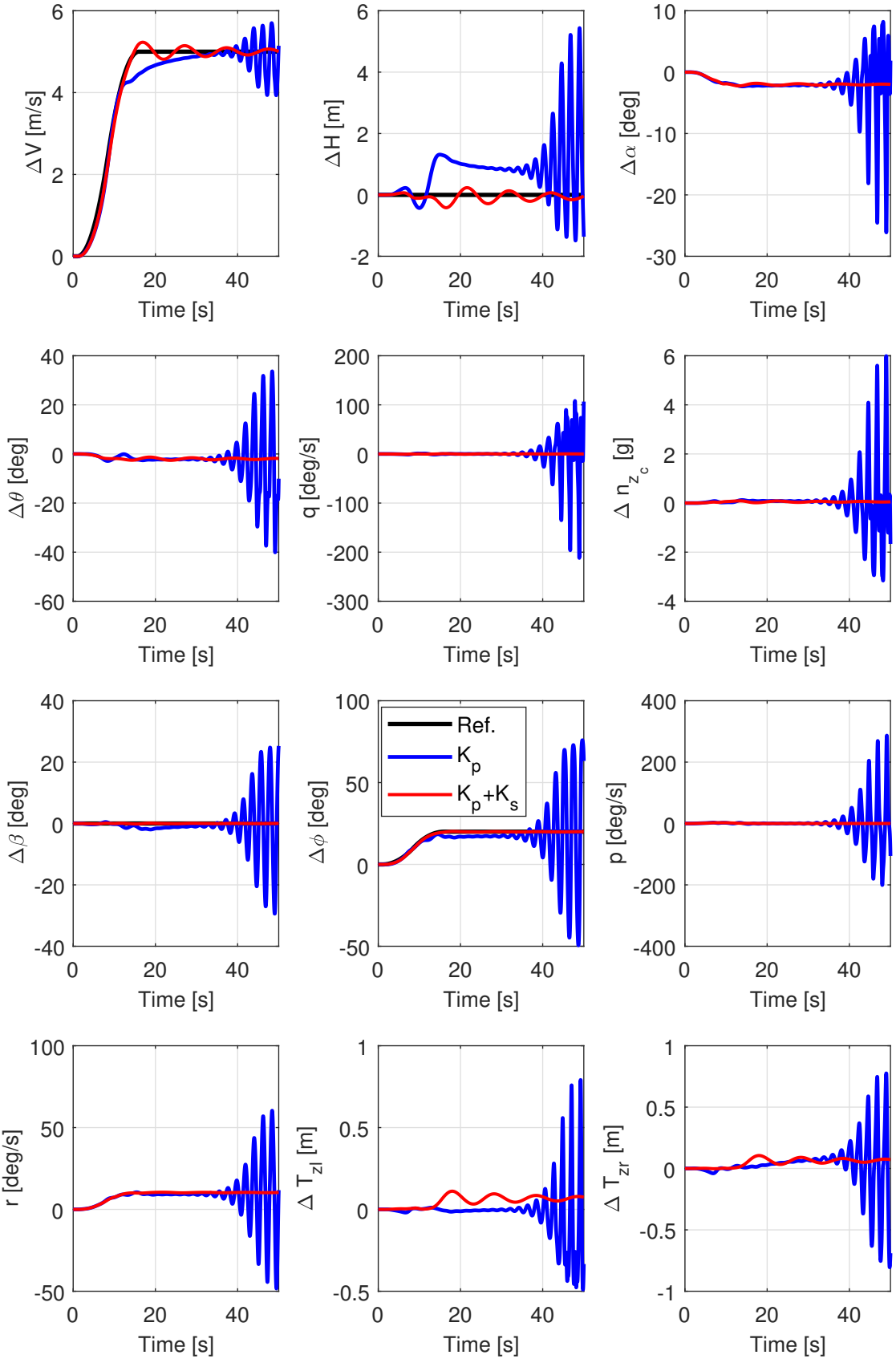

Figure 13: Longitudinal, vertical load factor, latero-directional measurements and wing tip displacements for a variation of 5m/s in a coordinated turn with fuzzy interpolation state-space matrices.

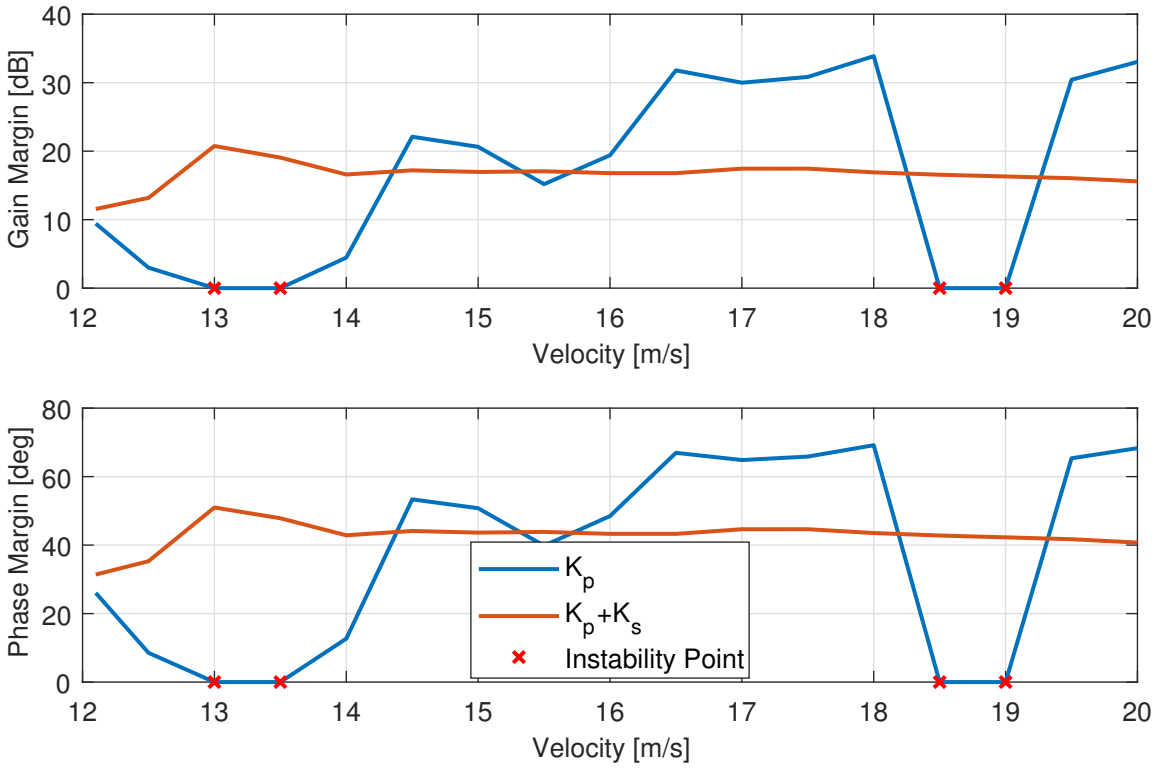

Figure 14: Gain and phase margins with and without the stabilizing gain.

5 CONCLUSION

A gain-scheduling approach based on fuzzy logic has been proposed in this paper to solve stability issues in flexible aircraft control. The approach combines closed-loop performance improvement via LQR and enforcement of stability in the whole flight envelope. One of its most relevant contributions is the enforcement of stability in a continuous envelope between design points, and not only for the design points themselves. Thus, there is an enormous potential of reducing the time necessary in the control law development, without the need to run several simulations (e.g. Monte-Carlo simulations) to look for stability issues in the entire envelope. Results comparing the proposed approach with traditional interpolation-based gain scheduling techniques showed that the present technique had overall a better performance, smoother closed-loop responses needing lower control surfaces deflections, and higher and more constant gain and phase margins in the entire velocity envelope.

So far the methodology covers only state feedback, however, it can be easily adapted to the design a Luenberger observer. The expansion of this method for output feedback is currently in progress.

6 FUNDING SOURCES

This study was financed in part by the Coordenação de Aperfeiçoamento de Pessoal de Nível Superior - Brasil (CAPES) - Finance Code 001.

Also the authors would like to thank the financial support from the Brazilian funding agency Financiadora de Estudos e Projetos FINEP and EMBRAER under grant number 01.14.0185.00.

7 REFERENCES

[1] Newsroom, F. (2016). Aquila's first flight: A big milestone toward connecting billions of people.

[2] Silvestre, F. J. and Luckner, R. (2015). Experimental validation of a flight simulation model for slightly flexible aircraft. *AIAA Journal*, 1–17.

[3] Guimarães Neto, A. B., Silva, R. G., Paglione, P., and Silvestre, F. J. (2016). Formulation of the flight dynamics of flexible aircraft using general body axes. *AIAA Journal*, 3516–3534.

[4] Waszak, M. R. and Schmidt, D. K. (1988). Flight dynamics of aeroelastic vehicles. *Journal of Aircraft*, 25(6).

[5] Shearer, C. M. and Cesnik, C. E. S. (2007). Nonlinear flight dynamics of very flexible aircraft. *Journal of Aircraft*, 44(5), 1528–1545.

[6] Cesnik, C. E. S., Senatore, P. J., Su, W., Atkins, E. M., and Shearer, C. M. (2012). X-hale: A very flexible unmanned aerial vehicle for nonlinear aeroelastic tests. *AIAA journal*, 50(12), 2820–2833.

[7] Silvestre, F. J., Neto, A. B. G. a., Bertolin, R. M., Silva, R. G. A. D., and Paglione, P. (2017). Aircraft control based on flexible aircraft dynamics. *Journal of Aircraft*, 54(1), 262–271.

[8] Gonzalez, P. J., Guimarães Neto, A. B., Chaves Barbosa, G., Bertolin, R. M., Silvestre, F. J., and Cesnik, C. E. S. (2017). X-hale autopilot with stability augmentation and shape control based on loop separation. In *International Forum on Aeroelasticity and Structural Dynamics*, 77. p. 19.

[9] Fan, W., Liu, H. H. T., and Kwong, R. H. S. (2017). Gain-Scheduling Control of Flexible Aircraft with Actuator Saturation and Stuck Faults. *Journal of Guidance, Control, and Dynamics*.

[10] Gonzalez, P. J., Silvestre, F. J., Paglione, P., Köthe, A., Pang, Z. Y., and Cesnik, C. E. (2016). Linear control of highly flexible aircraft based on loop separation. In *AIAA Atmospheric Flight Mechanics Conference,*. pp. 10.2514/6.2016–3398.

[11] Bertolin, R. M., Guimarães Neto, A. B., Barbosa, G. C., and Silvestre, F. J. (2018). Adaptive output-feedback gain scheduling applied to flexible aircraft. *31st Congress of the International Council of the Aeronautical Sciences, ICAS*.

[12] Alazard, D. (2002). Robust h design for lateral flight control of highly flexible aircraft. *Journal of Guidance, Control, and Dynamics*, 25(3), 502–509.

[13] Cesnik, C. E. S. and Su, W. (2011). Nonlinear aeroelastic simulation of x-hale: a very flexible uav. In *49th AIAA Aerospace Sciences Meeting including the New Horizons Forum and Aerospace Exposition, Orlando, Florida*.

[14] Cook, R. G., Palacios, R., and Goulart, P. (2013). Robust gust alleviation and stabilization of very flexible aircraft. *AIAA Journal*, 51(2), 330–340.

[15] Qu, Z., Annaswamy, A. M., and Lavretsky, E. (2016). Adaptive output-feedback control for a class of multi-input-multi-output plants with applications to very flexible aircraft. *2016 American Control Conference (ACC)*.

[16] Qu, Z. and Annaswamy, A. M. (2016). Adaptive output-feedback control with closed-loop reference models for very flexible aircraft. *Journal of Guidance, Control, and Dynamics*, 39(4), 873–888.

[17] Rugh, W. J. and Shamma, J. S. (2000). Research on gain scheduling. *Automatica*, 36(10), 1401–1425.

[18] Fujimori, A., Wu, Z., Nikiforuk, P., and Gupta, N. (1998). A design of alflex flight control system using fuzzy gain-scheduling. *AIAA Guidance, Navigation, and Control Conference*, 1739–1745.

[19] Gonsalves, P. G. and Zacharias, G. L. (1994). Fuzzy logic gain scheduling for flight control. In *Proceedings of 1994 IEEE 3rd International Fuzzy Systems Conference*. pp. 952–957 vol.2. doi:10.1109/FUZZY.1994.343863.

[20] Schram, G. (1998). *Intelligent flight control: A fuzzy logic approach*. Ph.D. thesis, Delft University of Technology. Thesis of Doctor in Science in Electrical Engineering, Mathematics and Computer Science.

[21] Barbosa, G. C., Bertolin, R., González, P. J., Guimarães Neto, A. B., and Silvestre, F. J. (2018). Fuzzy gain-scheduling applied for a very flexible aircraft. *AIAA Guidance, Navigation, and Control Conference, AIAA SciTech Forum*.

[22] Tanaka, K., Ikeda, T., and Wang, H. O. (1996). Robust stabilization of a class of uncertain nonlinear systems via fuzzy control: quadratic stabilizability, h^infty control theory, and linear matrix inequalities. *IEEE Transactions on Fuzzy Systems*, 4(1), 1–13. ISSN 1063-6706. doi:10.1109/91.481840.

[23] Stevens, B. L. and Lewis, F. L. (2003). *Aircraft Control and Simulation*. New Delhi: Wiley India, 2 nd ed. ISBN: 978-81-265-2567-6.

[24] Takagi, T. and Sugeno, M. (1985). Fuzzy identification of systems and its applications to modeling and control. *IEEE Transactions on Systems, Man, and Cybernetics*, SMC-15(1), 116–132. ISSN 0018-9472. doi:10.1109/TSMC.1985.6313399.

[25] Albano, E. and Rodden, W. P. (1969). A doublet-lattice method for calculating lift distributions on oscillating surfaces in subsonic flows. *AIAA journal*, 7(2), 279–285.

[26] Eversman, W. and Tewari, A. (1991). Consistent rational-function approximation for unsteady aerodynamics. *Journal of Aircraft*, 28(9), 545–552.

[27] LYAPUNOV, A. M. (1992). The general problem of the stability of motion. *International Journal of Control*, 55(3), 531–534.

[28] Tanaka, K. and Wang, H. O. (2001). *Fuzzy Control Systems Design and Analysis: a Matrix Inequality Approach*. John Wiley & Sons.

[29] Nesterov, Y. and Nemirovski, A. (1994). *Interior Point Polynomial Methods in Convex Programming: Theory and Applications*. SIAM.

[30] Mozelli, L., Palhares, R., Souza, F., and Mendes, E. (2009). Reducing conservativeness in recent stability conditions of ts fuzzy systems. *Automatica*, 45(6), 1580–1583.

[31] Mozelli, L. A., Campos, C. D., Palhares, R. M., Tôrres, L. A. B., and Mendes, E. M. A. M. (2007). Chaotic synchronization and information transmission experiments: a fuzzy relaxed h∞ control approach. *Circuits, Systems, and Signal Processing*, 26(4), 427–449.

[32] Nguyen, A.-T., Márquez, R., Guerra, T.-M., and Dequidt, A. (2017). Improved lmi conditions for local quadratic stabilization of constrained takagi-sugeno fuzzy systems. *International Journal of Fuzzy Systems*, 19(1), 225–237.

[33] Guimarães Neto, A. B. (2014). *Flight dynamics of flexible aircraft using general body axes: a theoretical and computational study*. Ph.D. thesis, Instituto Tecnológico de Aeronáutica, São José dos Campos. Thesis of Doctor in Science in Flight Mechanics.

[34] Eugene, L., Kevin, W., and Howe, D. (2013). *Robust and adaptive control with aerospace applications*. Springer London.

COPYRIGHT STATEMENT